X-ray Structural Studies on a Series of Oxygenated Anthracene Cycloadducts. Evidence for $\pi-\sigma^*$ Negative Homohyperconjugation in the Ground State

Brett R. Pool, Jonathan M. White,* and P. Peter Wolynec

School of Chemistry University of Melbourne, Parkville VIC 3010, Australia

j.white@chemistry.unimelb.edu.au

Received June 30, 2000

Application of the variable oxygen probe to low-temperature crystal data from the series of oxygenated anthracene cycloadducts **10**−**16**, revealed a strong response of the C−OR bond distance in these structures to the electron demand of the OR group. It is believed that this represents the manifestation of $\pi-\sigma^*$ negative homohyperconjugation in the ground state. Ab initio molecular orbital calculations on the model system **18** provided further support for this.

Introduction

Participation by neighboring π systems in reactions involving carbenium ion intermediates has been demonstrated in many studies.[1−4] Evidence has been provided by solvolysis studies where enhancements in reaction rates are often observed,[2] stereochemical studies where solvolysis occurs with retention of absolute or relative configuration,[3,4] and by the frequent observation of rearranged products in many solvolysis reactions.[1−4] For example solvolysis of tosylate **1** in aqueous acetic acid (Scheme 1)[1] has been reported to result in the formation of the rearranged alcohols **2** and **3**.

A likely mechanism for the formation of **2** and **3** is depicted in Scheme 2. The first step involves displacement of the leaving group by the neighboring π system giving the intermediate phenylium ion **4**, which is either captured by water (path a) giving the endo alcohol **2**, or survives long enough (path b) to give the benzylic cation **5**. Capture of **5** can be expected to give both the endo **2** and exo **3** alcohols. An alternative mechanism, involving unassisted heterolysis of the C−OTs bond followed by phenyl ring participation, cannot be discounted without labeling studies. However if the mechanism depicted in Scheme 2 is correct, then the early stages of this reaction will involve interaction between the π electron density in the benzene ring anti to the tosylate leaving group with the σ^* orbital of the C−OTs bond. This through-space homohyperconjugative interaction would be expected to facilitate the departure of the leaving group. We were intrigued to determine whether the $\pi-\sigma^*$ interaction (Figure 1) implied by this mechanism could be detected in the ground state from a systematic X-ray structural study of esters and ethers derived from the alcohol **6**. Such a study would also shed some light on the mechanism of this rearrangement.

The *variable oxygen probe* is an X-ray structural method for detecting the presence of electronic interactions between electron donors and oxygenated substituents in the ground state. Kirby and Jones et al. established that the C−O bond distance in the C−OR fragment increases with increasing electron demand of the OR substituent; this correlation reflects an increasing contribution of the C^+ $^-$OR valence bond form to the ground-state structure.[5,6] If the electron demand of a substituent OR is quantified as the pK_a value for the parent acid

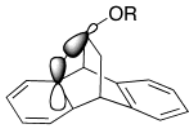

6; R = H

Figure 1. $\pi-\sigma^*$ interaction.

Scheme 1

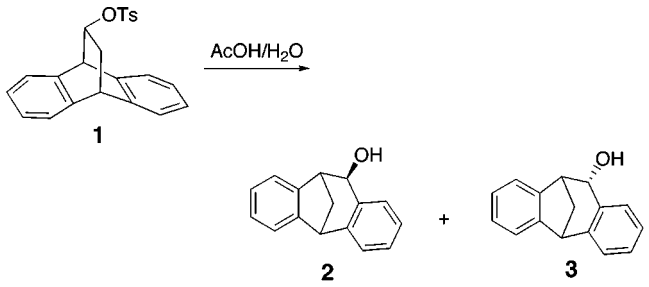

Scheme 2

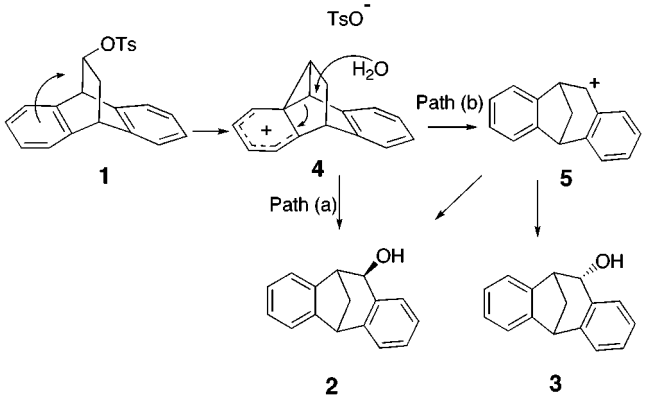

* To whom correspondence should be addressed.

(1) Stanescu, M. D.; Florea, C.; Chiraleu, F.; Hirtopeanu, A.; Sezonov, P. *Rev. Roum. Chim.* **1998**, *43*, 861.

(2) Allred, E. L.; Hinshaw, J. C. *Tetrahedron Lett.* **1968**, 1293.

(3) Brown, H. C.; Kim, C. J.; Lancelot, C. J.; Schleyer, P. v. *J. Am. Chem. Soc.* **1970**, *92*, 5244. Brown, H. C.; Kim, C. J. *Ibid.* **1971**, *93*, 5765.

(4) Shoppee, C. W. *J. Chem. Soc.* **1946**, 1147.

10.1021/jo0055638 CCC: $19.00
Published on Web 10/05/2000

Table 1. Selected Bond Distances (Å) and Angles (deg) for Compounds 10−16

	10	11	12	13	14	15	16
			Distances				
C11−O1	1.456(2)	1.466(2)	1.476(2)	1.455(1)	1.438(2)	1.460(2)	1.462(2)
C9−C11	1.550(3)	1.546(2)	1.540(2)	1.550(2)	1.545(2)	1.545(3)	1.545(3)
C10−C12	1.554(3)	1.558(2)	1.555(2)	1.561(2)	1.554(2)	1.563(3)	1.553(3)
C11−C12	1.534(3)	1.545(3)	1.542(3)	1.541(2)	1.545(2)	1.541(3)	1.540(3)
C8a···.C11	2.429(3)	2.413(3)	2.447(3)	2.439(2)	2.423(2)	2.418(3)	2.429(3)
C1a−C9	1.512(2)	1.514(2)	1.516(2)	1.511(2)	1.509(2)	1.517(3)	1.511(3)
C8a−C9	1.517(3)	1.509(3)	1.516(2)	1.517(2)	1.515(2)	1.518(3)	1.518(2)
C4a−C10	1.514(3)	1.513(2)	1.515(2)	1.516(2)	1.515(2)	1.516(3)	1.516(2)
C5a−C10	1.509(3)	1.515(3)	1.514(3)	1.516(2)	1.507(2)	1.516(3)	1.512(3)
C1a−C1	1.382(3)	1.382(3)	1.386(3)	1.383(2)	1.384(2)	1.383(3)	1.384(3)
C1−C2	1.391(3)	1.390(3)	1.395(3)	1.391(2)	1.388(2)	1.397(4)	1.387(3)
C2−C3	1.390(3)	1.388(3)	1.385(3)	1.387(2)	1.386(3)	1.380(4)	1.383(3)
C3−C4	1.389(3)	1.391(3)	1.387(3)	1.394(2)	1.392(2)	1.399(4)	1.385(3)
C4−C4a	1.387(3)	1.385(2)	1.389(3)	1.388(2)	1.384(2)	1.383(3)	1.388(3)
C1a−C4a	1.399(3)	1.399(3)	1.397(3)	1.401(2)	1.401(2)	1.401(3)	1.395(3)
C5a−C5	1.381(3)	1.386(3)	1.388(3)	1.386(2)	1.389(2)	1.390(3)	1.380(3)
C5−C6	1.387(3)	1.388(3)	1.394(3)	1.393(2)	1.388(3)	1.397(4)	1.376(3)
C6−C7	1.383(3)	1.389(3)	1.385(3)	1.388(2)	1.382(3)	1.385(4)	1.378(4)
C7−C8	1.395(3)	1.388(3)	1.391(3)	1.395(2)	1.395(2)	1.396(3)	1.395(3)
C8−C8a	1.380(3)	1.389(3)	1.385(3)	1.386(2)	1.383(2)	1.384(3)	1.388(3)
C5a−C8a	1.396(3)	1.399(3)	1.399(3)	1.401(2)	1.398(2)	1.395(3)	1.398(3)
C13−O2	1.199(2)	1.194(2)	*	1.207(1)	*	1.203(3)	1.200(2)
			Angles				
C9−C11−O1	109.3(2)	110.3(1)	107.7(1)	112.2(1)	105.6(1)	104.6(2)	104.8(1)
C1a−C9−C11	107.2(2)	107.0(2)	107.0(1)	106.8(1)	107.0(1)	108.0(2)	105.8(2)
C8a−C9−C11	104.7(2)	104.4(1)	106.4(1)	105.3(1)	104.7(1)	104.3(2)	105.1(1)
C1a−C9−C8a	108.0(2)	108.9(1)	106.6(1)	107.8(1)	108.2(1)	108.1(2)	109.9(2)
C4a−C10−C12	106.5(2)	105.9(2)	106.5(1)	107.1(1)	106.8(1)	106.6(2)	106.4(2)
C5a−C10−C12	106.1(2)	106.5(1)	107.1(1)	105.4(1)	105.8(1)	106.4(2)	105.1(2)
C4a−C10−C5a	107.8(2)	107.7(1)	106.5(1)	107.5(1)	107.7(1)	107.4(2)	108.5(2)

(R−OH), then a plot of C−OR distance vs pK_a of ROH is linear, and the slope of the resulting plot is sensitive to the effects of electron donation into the C−OR σ^* antibonding orbital. The presence of good donor orbitals vicinal and antiperiplanar to the OR bond results in a strong response of the C−OR distance to the electron demand of OR, resulting from increased stabilization of the cation part of the valence bond form $C^{+}\ ^{-}OR$. For example, the plots of C−OR bond distance vs pK_a (ROH) constructed for **7**,[5] **8**,[7] and **9**[6] give the following relationships:

$$\mathbf{7}\ r(\mathrm{C{-}O}),\ \text{Å} = 1.475 - (2.9 \times 10^{-3})\ \mathrm{p}K_a\ (\mathrm{R'OH}) \quad (1)$$

$$\mathbf{8}\ r(\mathrm{C{-}O}),\ \text{Å} = 1.502 - (5.3 \times 10{-}3)\ \mathrm{p}K_a\ (\mathrm{ROH}) \quad (2)$$

$$\mathbf{9}\ r(\mathrm{C{-}O}),\ \text{Å} = 1.493 - (6.5 \times 10{-}3)\ \mathrm{p}K_a\ (\mathrm{R'OH}) \quad (3)$$

A strong response of C−OR bond distance to the

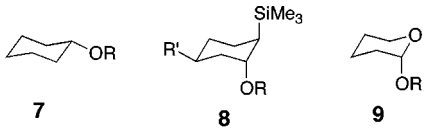

7 **8** **9**

electron demand of OR is demonstrated for **9** which has oxygen lone pair (n_O) orbital antiperiplanar to the OR substituent (this is the basis of the well-known anomeric effect). A strong response is also observed for **8** which has a C−Si bond antiperiplanar to the OR substituent (this is the basis of the silicon β-effect). However, a weaker response is obvious in **7** which has σ_{c-c} bonding orbital, which is a weaker donor orbital, antiperiplanar to the OR bond.

The aim of this work was to determine whether the variable oxygen probe could be used to provide evidence for the $\pi-\sigma^*$ in the ground-state structures of the oxygenated anthracene cycloadducts **10**−**16**.

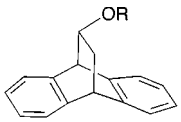

10; R = $COCH_3$
11; R = $COCCl_3$
12; R = SO_2CH_3
13; R = PhCO
14; R = *p*-NO_2Ph
15; R = *p*-NO_2PhCO
16; R = 3,5-$(NO_2)_2$PhCO

Results and Discussion

Synthesis. The parent alcohol **6** was found to be most readily prepared by lithium aluminum hydride reduction of the anthracene−vinyl acetate cycloadduct **10**.[8] The ester and ether derivatives **11**−**16** which cover a pK_a range (ROH) of 7.15 (for **14**) down to −1.9 (for **12**) were prepared from **6** using standard techniques and reagents.

Molecular Structures. Structures were determined at low temperature to minimize the effects of thermal motion, Structures **10**, **12**−**15** were determined at 130 K while **11** and **16** which underwent destructive phase changes upon cooling to this temperature were determined at 200 and 220 K, respectively. Selected structural parameters for **10**−**16** are presented in Table 1 while a

(5) Amos, R. D.; Handy, N. C.; Jones, P. G.; Kirby, A. J.; Parker, J. K.; Percy, J. M.; Su, M. D. *J. Chem. Soc., Perkin Trans. 2* **1992**, 549.
(6) Briggs, A. J.; Glenn, R.; Jones, P. G.; Kirby, A. J.; Ramaswamy, P. *J. Am. Chem. Soc.* **1984**, *106*, 6200.
(7) Giordano, J.; Green, A. J.; White, J. M. *Aust. J. Chem*. **2000** *53*, 285.
(8) Chung Y.; Duerr B. F.; McKelvey T. A.; Nanjappan P.; Czarnik A. W. *J. Org. Chem*. **1989**, *54*, 1018.

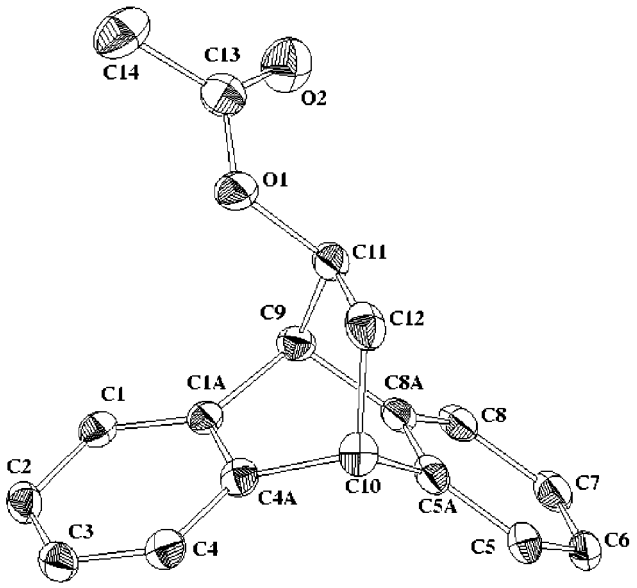

Figure 2. Thermal ellipsoid plot of compound **10**.

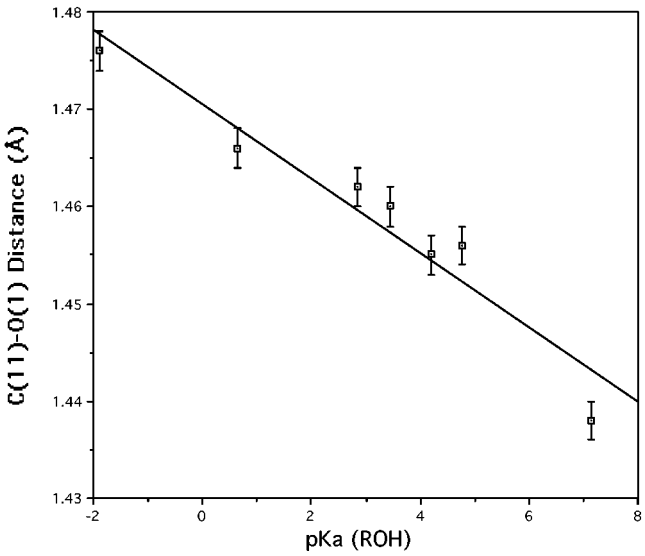

Figure 3. Plot of C(11)−O(1) distance vs pK_a (ROH) for compounds **10**−**16**.

perspective diagram for one of these (**10**) is presented in Figure 2. A plot of the C−OR bond distance vs pK_a (ROH) is presented in Figure 3. From this plot the following relationship between the C(11)−OR distance and pK_a (ROH) was determined:

$$r(\text{C}-\text{OR}),\ \text{Å} = 1.470 - (3.8 \times 10^{-3})\ \text{p}K_a\ (\text{ROH})\ (R = 0.94) \quad (4)$$

The slope of this plot which is -3.8×10^3, not surprisingly, indicates a weaker response of C−OR bond distance to the electron demand of OR than was observed in the strong donor systems **8** and **9**. However, the slope does represent a significantly stronger response than was observed in the simple cyclohexyl derivatives **7**. It can be argued that the stronger response of the C−OR distance to the electron demand of the OR substituent in **6** and its derivatives compared with **7** arises from a ground state $\pi-\sigma^*$ interaction. This argument is based

Figure 4. Possible interactions involving the C−OR σ^* orbital.

on the fact that, besides the π orbitals in the aromatic ring which is anti to the OR substituent, the only other orbital which overlaps effectively with the C−OR σ^* antibonding orbital is the vicinal C−C bonding orbital (Figure 4).

Given that a weaker response of C−OR distance to pK_a (ROH) is observed in **7** (slope = 2.9) which has two σ_{C-C} bonds overlapping with the σ^*_{C-OR} orbital, and given that the vicinal C−C bond in **6** and its derivatives should be an even weaker electron donor than the C−C bonds in **7** (due to the presence of one sp^2 hybridized carbon) then the strong response of C−OR bond distance in **6** and its derivatives to the electron demand of OR must reflect the effects of the $\pi-\sigma^*$ interaction. Given that these plots are based on logarithms, then these data imply that phenyl participation in **1** is an order of magnitude stronger than C−C participation in **7**.

The strength of the $\sigma-\pi$ interaction in **6** and its derivatives is expected to increase with increasing electron demand of the OR substituent (due to the lowering of the energy of σ^*_{C-OR} orbital leading to a better energy match with the π orbital). In valence bond terms this implies an increasing contribution of the resonance form **17** to the ground-state structure of **6** and its derivatives.

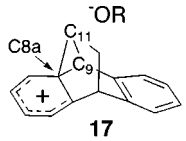

17

Increasing contributions of **17** to the ground-state structure might be expected to lead to observable changes to the C(8a)−C(9)−C(11) angle and concomitant contraction of the C(8a)···C(11) distance with increasing electron demand of the OR substituent and perhaps systematic variations of the C−C bond distances within the "donor" ring. However, when these structural parameters were plotted against the pK_a value (ROH) for each structure **10**−**16**, no clear trends were apparent. This result might suggest that variations in these parameters were too small to be observable by X-ray crystallography; this interpretation is supported by ab initio calculations (below).

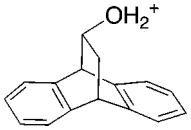

18

To gain further evidence and insight into the $\pi-\sigma^*$ interaction in **10**−**16**, ab initio molecular orbital calculations were carried out on the model compound **18** in which the leaving group is H_2O. This system was chosen so that the $\pi-\sigma^*$ interaction would not result in a

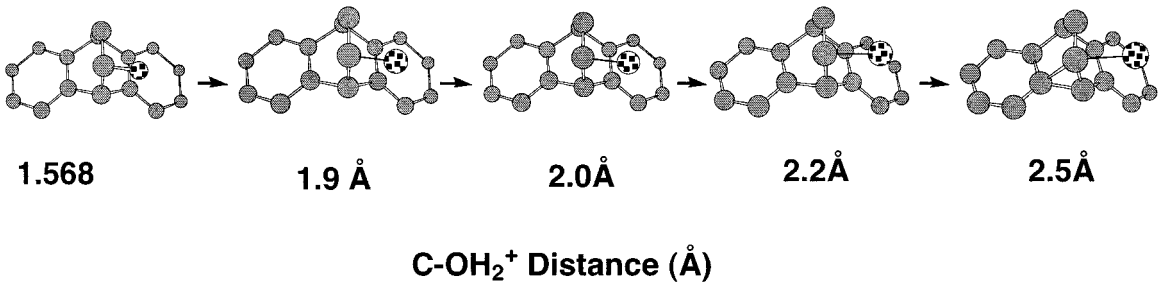

Figure 5. Calculated reaction coordinate for heterolysis of the C−OH_2^+ bond in **18**.

Table 2. Summary of Calculated Geometrical Data, Atomic Charges, and Bond Populations for 18

				Distances					
C(12)−O(1)	1.568	1.618	1.668	1.718	1.768	1.900	2.000	2.200	2.499
C(1a)-C(4a)	1.398	1.397	1.397	1.397	1.397	1.394	1.393	1.393	1.378
C(1a)-C(1)	1.384	1.383	1.383	1.382	1.381	1.381	1.381	1.381	1.392
C(1)−C(2)	1.393	1.393	1.393	1.393	1.393	1.393	1.392	1.391	1.390
C(2)−C(3)	1.382	1.383	1.383	1.382	1.383	1.383	1.384	1.384	1.396
C(3)−C(4)	1.394	1.393	1.393	1.393	1.392	1.392	1.392	1.391	1.391
C(4)−C(4a)	1.378	1.378	1.379	1.379	1.379	1.380	1.379	1.380	1.380
C(5)−C(6)	1.391	1.391	1.391	1.391	1.391	1.391	1.390	1.390	1.376
C(5)−C(5a)	1.379	1.379	1.380	1.380	1.379	1.380	1.380	1.380	1.402
C(6)−C(7)	1.385	1.384	1.384	1.384	1.385	1.385	1.387	1.389	1.390
C(7)−C(8)	1.390	1.390	1.389	1.390	1.389	1.388	1.388	1.384	1.379
C(8a)-C(5a)	1.392	1.393	1.393	1.392	1.393	1.393	1.393	1.395	1.518
C(8a)-C(8)	1.379	1.380	1.380	1.380	1.381	1.382	1.383	1.388	1.402
C(9)−C(1a)	1.521	1.521	1.521	1.521	1.520	1.519	1.518	1.514	1.579
C(9)−C(8a)	1.521	1.522	1.525	1.526	1.528	1.533	1.537	1.548	1.546
C(9)−C(11)	1.535	1.530	1.526	1.521	1.516	1.502	1.492	1.468	1.430
C(10)−C(5a)	1.520	1.520	1.520	1.520	1.520	1.521	1.521	1.522	1.503
C(10)−C(4a)	1.519	1.519	1.519	1.518	1.518	1.519	1.518	1.518	1.520
C(10)−C(12)	1.554	1.554	1.554	1.553	1.554	1.553	1.551	1.550	1.868
C(12)−C(11)	1.537	1.534	1.530	1.527	1.524	1.516	1.511	1.503	1.513
C(8a)···C(11)	2.414	2.400	2.387	2.373	2.357	2.311	2.27	2.162	1.868
C(8a)−C(9)−C(11)	104.3°	103.7°	103.0°	102.3°	101.5°	99.2°	97.0°	91.5°	76.6°
				Charges[a]					
O	0.297	0.274	0.253	0.231	0.211	0.158	0.122	0.066	0.028
C(1)	−0.001	−0.002	−0.002	−0.003	−0.003	−0.002	−0.001	0.005	0.017
C(2)	0.043	0.043	0.043	0.042	0.042	0.041	0.039	0.037	0.036
C(3)	0.050	0.050	0.049	0.049	0.049	0.048	0.047	0.047	0.047
C(4)	0.018	0.017	0.017	0.017	0.017	0.016	0.016	0.016	0.015
C(5)	0.008	0.009	0.009	0.010	0.010	0.012	0.012	0.014	0.009
C(5a)	0.053	0.055	0.058	0.060	0.064	0.074	0.084	0.114	0.198
C(6)	0.048	0.049	0.050	0.052	0.053	0.059	0.064	0.078	0.125
C(7)	0.034	0.034	0.035	0.035	0.035	0.036	0.036	0.036	0.029
C(8)	0.020	0.022	0.024	0.027	0.029	0.037	0.043	0.062	0.131
C(8a)	0.015	0.009	0.002	−0.005	−0.013	−0.037	−0.059	−0.116	−0.250
				Population					
C(11)···C(8a)	−0.080	−0.079	−0.078	−0.077	−0.076	−0.069	−0.060	−0.034	0.059

[a] Charges include contributions from attached hydrogens.

separation of charges which might be disfavored in these gas-phase calculations. The ground-state structure of **18** was calculated at the RHF 631-G* level of theory. Optimization of **18** using the 6-31 G** basis set did not lead to any significant changes in geometry, therefore the RHF/631 G* basis set was used for the remainder of these calculations. The C−OH_2 bond distance was then systematically lengthened from 1.568 Å (as optimized RHF/631 G*) to 2.5 Å in order to examine how the $\pi-\sigma^*$ interaction would manifest along the reaction coordinate leading toward heterolysis of the C−OH_2^+ bond (Figure 5). Attempts to extend the C−OH_2^+ distance beyond 2.5 Å were not practical due to excessive calculation times without convergence.

A summary of selected bond distances, angles, atomic charges, and electron populations is presented in Table 2. An inspection of Table 2 shows that as the C−OH_2^+ bond is lengthened there is a concomitant decrease in the C(8a)−C(9)−C(11) angle and in the associated C(8a)···C(11) distance. A plot of the bonding electron population density between C(8a) and C(11) vs the C−OH_2^+ bond distance (Figure 6) clearly shows that electron density between these two nuclei increases as the C−OH_2^+ bond is broken, consistent with the development of bonding character between these two nuclei. An analysis of selected atomic charge densities (Figure 7) shows a steady increase in positive charge at C(5a), C(6), and C(8) and a steady decrease in the positive charge on the oxygen; atomic charge densities on C5, C7, C(1)−C(4) vary also but to a much smaller extent. These effects are consistent with the smooth formation of the phenylium ion intermediate **4** as the OH_2^+ group departs. Interestingly the C−C bond distances within the participating benzene ring (Figure 8) do not show any significant variation until the C−OH_2^+ is extended to 2.2−2.5 Å this result sheds some light on the X-ray data above where

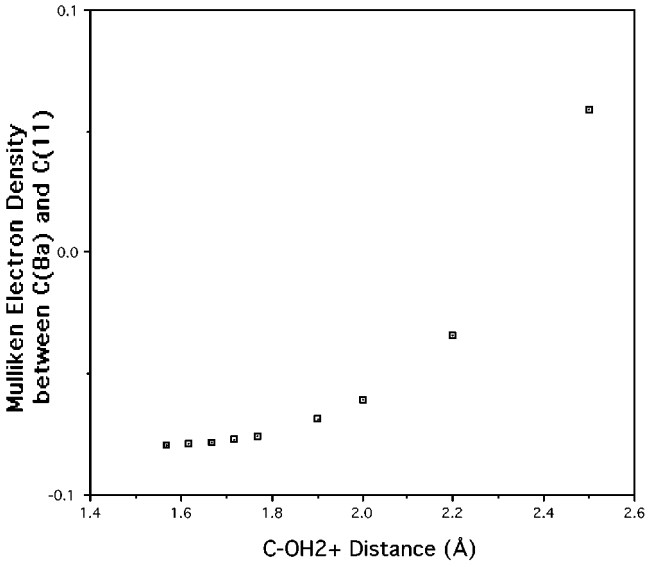

Figure 6. Population density between C(8a) and C(11) as a function of the C−OH2+ distance.

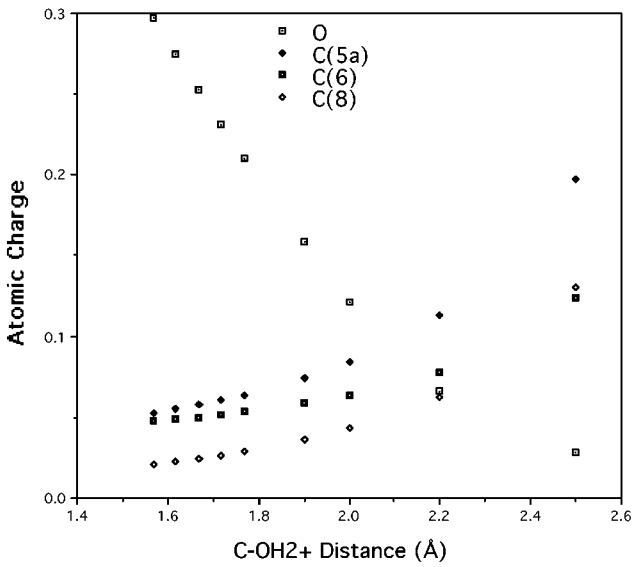

Figure 7. Plot of selected atomic charges vs the C(11)−O distance.

we observed that the same C−C distances showed no significant variation with the electron demand of the ester group in structures **10**−**16**.

Conclusion

The X-ray structural data on the anthracene cycloadducts **10**−**16** provide evidence for a $\pi-\sigma^*$ interaction involving the benzene ring anti to the oxygen leaving group and the C−O antibonding orbital in the ground state. Calculations on the model compound **18** show that heterolysis of the C−O bond leads smoothly to a phenylium ion intermediate. Although neighboring group effects are likely to be overemphasized in gas-phase calculations, both the X-ray structural data and the ab initio calculations provide evidence that heterolysis of the C−OTs bond in **1** (Scheme 2) does indeed lead smoothly to the intermediate **4** rather than an unassisted heterolysis step followed by phenyl ring participation.

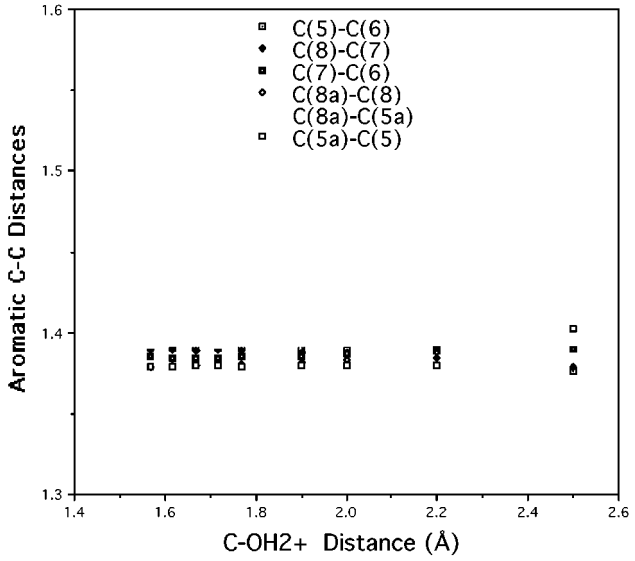

Figure 8. Plot of selected C−C distances vs C−OH2+ distance (Å).

Experimental Section

(a) Crystallography. Diffraction data were recorded on an Enraf Nonius CAD4f diffractometer operating in the $\theta/2\theta$ scan mode at low temperature (130.0 K) **10**, **12**−**15** and 200 K for **11** and 220 K for **16**. Crystal data and structure refinement details for **10**−**16** are presented in Table 3. The crystals were flash-cooled prior to setup and data collection. Unit cell dimensions were corrected for any θ zero errors by centering reflections at both positive and negative θ angles. The data were corrected for Lorentz and polarization effects[9] for absorption (Analytical correction within SHELX 76)[10] and extinction.[11] Structures were solved by direct methods (SHELXS-86)[12] and were refined on F^2 (SHELXL-97).[11] Thermal ellipsoid plots were drawn using the program ZORTEP.[13]

(b) Ab Initio Calculations. All ab initio calculations were performed on a "farm" of DEC 600 workstations using the Gaussian 94 suite of programs.[14,15]

(c) Synthesis. General experimental details including solvent purification procedures and NMR acquisitions are as reported in a previous paper.[16]

Preparation of the Anthracene Vinyl Acetate Cycloadduct 10. Anthracene (1.60 g, 8.98×10^{-3}mol) and vinyl acetate (3.5 mL, 3.80×10^{-2}mol) were placed in xylene (20 mL) in a sealed test tube. The mixture was heated for 45 h at 230 °C in a fluidized sand bath. After removal of the majority of the xylene under reduced pressure, the residue was recrys-

(9) Gable, R. W.; Hoskins, B. F.; Linden, A.; McDonald, I. A. S.; Steen, R. J. *Process_data*; Program for Processing of CAD-4 Diffractometer Data. University of Melbourne, Australia, 1994.
(10) SHELX76: Sheldrick, G. M. *Program for Crystal Structure Determination*; Cambridge, England, 1976.
(11) SHELXL-97: Sheldrick, G. M. *Program for Crystal Structure Refinement;* University of Göttingen, Germany, 1997.
(12) SHELXS-86: Sheldrick, G. M. *Crystallographic Computing 3*;
(13) Zsolnai, L. ZORTEP, *An Interactive ORTEP Program*; University of Heidelberg, Germany, 1994.

(14) Gaussian 94, Revision E.2, Frisch, M. J.; Trucks, G. W.; Schlegel, H. B.; Gill, P. M. W.; Johnson, B. G.; Robb, M. A.; Cheeseman, J. R.; Keith, T.; Petersson, G. A.; Montgomery, J. A.; Raghavachari, K.; Al-Laham, M. A.; Zakrzewski, V. G.; Ortiz J. V.; Foresman, J. B.; Cioslowski, J.; Stefanov, B. B.; Nanayakkara, A.; Challacombe, M.; Peng, C. Y.; Ayala, P. Y.; Chen, W.; Wong,. M. W.;. Andres, J. L.; Replogle, E. S.; Gomperts, R.; Martin, R. L.; Fox, D. J.; Binkley, J. S.; Defrees, D. J.; Baker, J.; Stewart, J. P.; Head-Gordon, M.; Gonzalez, C.; Pople, J. A. Gaussian, Inc., Pittsburgh, PA, 1995.
(15) Roothaan, C. C. J. *Rev. Mod. Phys.* **1951**, *23*, 69.
(16) White, J. M.; Robertson, G. B. *J. Org. Chem*. **1992**, *57*, 4638.

Table 3. Crystal Data and Refinement Details for Compounds 10−16

compound	**10**	**11**	**12**	**13**	**14**	**15**	**16**
empirical formula	$C_{18}H_{16}O_2$	$C_{18}H_{13}Cl_3O_2$	$C_{17}H_{15}O_3S$	$C_{23}H_{18}O_2$	$C_{22}H_{17}NO_3$	$C_{23}H_{17}NO_4$	$C_{23}H_{16}N_2O_6$
formula weight	264.31	367.63	299.35	326.37	343.37	371.38	416.38
temperature (K)	130.0(1)	200.0(1)	130.0(1)	130.0(1)	130.0(1)	130.0(1)	220.0(1)
radiation	Mo Kα	Mo Kα	Mo Kα	Cu Kα	Cu Kα	Cu Kα	Cu Kα
wavelength (Å)	0.71069	0.71069	0.71069	1.5418	1.5418	1.54180	1.54180
crystal system	triclinic	monoclinic	monoclinic	monoclinic	monoclinic	monoclinic	monoclinic
space group	*P*-1	$P2_1/n$	$P2_1/n$	$P2_1/n$	$P2_1/n$	$P2_1$	$P2_1/c$
unit cell dimensions							
a (Å)	7.6330(10)	11.8159(8)	6.276(3)	15.6340(13)	8.898(2)	9.1810(10)	12.365(3)
b (Å)	11.9250(10)	6.2448(4)	27.337(4)	6.1917(4)	17.151(2)	8.0891(4)	9.3350(10)
c (Å)	15.969(3)	22.312(3)	8.349(3)	16.9234(2)	11.194(2)	12.480(2)	17.408(4)
α (deg)	81.360(10)						
β (deg)	77.27(2)	97.906(7)	100.72(3)	97.445(8)	94.37(2)	106.245(7)	103.96(2)
γ (deg)	78.525(8)						
volume ($Å_3$)	1380.9(3)	1630.7(2)	1407.4(9)	1624.39(17)	1703.3(5)	889.84(18)	1950.0(7)
Z	4	4	4	4	4	2	4
D_c (g/cm_3)	1.271	1.497	1.413	1.335	1.339	1.386	1.418
μ (mm^{-1})	0.082	0.568	0.237	0.662	0.722	0.779	0.871
F(000)	560	752	628	688	720	388	864
crystal size (mm)	0.3 × 0.2 × 0.2	0.4 × 0.4 × 0.3	0.5 × 0.3 × 0.2	0.5 × 0.25 × 0.05	0.35 × 0.2 × 0.1	0.2 × 0.13 × 0.13	0.25 × 0.15 × 0.15
θ range (deg)	2.07−25.01	2.08−27.49	2.59−27.44	3.62−74.91	4.73−75.25	3.69−75.06	3.68−74.96
index ranges	$0 \le h \le 9$	$0 \le h \le 15$	$0 \le h \le 8$	$0 \le h \le 19$	$-11 \le h \le 0$	$-11 \le h \le 11$	$0 \le h \le 15$
	$-13 \le k \le 14$	$0 \le k \le 8$	$0 \le k \le 35$	$-7 \le k \le 0$	$0 \le k \le 21$	$-10 \le k \le 0$	$-11 \le k \le 0$
	$-18 \le l \le 18$	$-28 \le l \le 28$	$-10 \le l \le 10$	$-21 \le l \le 21$	$-13 \; l \le 14$	$0 \le l \le 140 \le l \le 15$	$-21 \le l \le 21$
no. intensity controls	3	3	3	3	3	3	3
interval (min)	160	160	160	160	160	160	160
decomposition	<2%	<2%	<2%	<2%	<2%	<2%	<2%
reflections collected	5245	3911	3492	3342	3735	2062	4201
independent reflections	4848	3734	3205	3227	3513	1975	4011
R_{int}	0.0238	0.0177	0.0158	0.0208	0.0558	0.0147	0.0206
observed ($I > 2\sigma(I)$)	3677	2923	2520	2856	3085	1802	3025
data/restraints/params	4848/0/490	3734/0/261	3205/0/255	3227/0/299	3513/0/304	1975/1/322	4011/0/329
goodness-of-fit on F^2	1.016	1.024	1.059	1.058	1.071	1.029	1.029
final *R* indices ($I > 2\sigma(I)$)	$R_1 = 0.0427$	$R_1 = 0.0407$	$R_1 = 0.0394$	$R_1 = 0.0330$	$R_1 = 0.0424$	$R_1 = 0.0309$	$R_1 = 0.0441$
	$wR_2 = 0.0993$	$wR_2 = 0.0994$	$wR_2 = 0.0905$	$wR_2 = 0.0881$	$wR_2 = 0.1132$	$wR_2 = 0.0777$	$wR_2 = 0.1185$
R indices (all data)	$R_1 = 0.0643$	$R_1 = 0.0579$	$R_1 = 0.0582$	$R_1 = 0.0382$	$R_1 = 0.0488$	$R_1 = 0.0366$	$R_1 = 0.0631$
	$wR_2 = 0.1110$	$wR_2 = 0.1102$	$wR_2 = 0.0992$	$wR_2 = 0.0920$	$wR_2 = 0.1187$	$wR_2 = 0.0817$	$wR_2 = 0.1309$
absolute structure parameter							
weighting scheme:							
$w = 1/[\sigma^2(F_o^2) + (A*P)^2 + B*P]$,	$A = 0.0578$	$A = 0.0586$	$A = 0.0413$	$A = 0.0497$	$A = 0.0608$	$A = 0.0509$	$A = 0.708$
where $P = (F_o^2 + 2F_c^2)/3$	$B = 0.4592$	$B = 0.6267$	$B = 0.7108$	$B = 0.4124$	$B = 0.6088$	$B = 0.0917$	$B = 0.3881$
extinction coefficient	0.0087(16)	0.0093(12)	0.0031(12)	0.0037(4)	0.0008(3)	0.0069(9)	0.0019(3)
maximum shift/esd	0.001		0	0	0	0.001	0.017
diff peak and hole (e $Å^{-3}$)	0.239, −0.217	0.357, −0.370	0.311, −0.300	0.264, −0.144	0.335, −0.251	0.211, −0.142	0.185, −0.223

tallized from methanol to afford pure **10** (1.21 g, 51%). mp 98−99 °C (lit.[8] 100−101).

Preparation of Alcohol 6. A solution of **10** (3.68 g, 1.39 × 10^{-2}mol) in dry ether (40 mL) was added dropwise to a slurry of lithium aluminum hydride (0.65 g, 1.71 × 10^{-2}mol) in dry ether (15 mL) under nitrogen at 0 °C. The resulting mixture was stirred for 14 h. After destroying the excess reagent by the careful addition of water, the mixture was filtered through Celite. The filtrate was separated, the organic layer dried with $MgSO_4$, and the solvent removed under reduced pressure to yield crude **6** which was recrystallized from methanol (2.64 g, 85%). mp 140−141 °C (lit.[8] 140−141 °C).

General Procedure for the Preparation of Ester Derivatives of 6. Alcohol **6** (0.30 g, 1.35 × 10^{-3} mol) was stirred in pyridine (5 mL) at 0 °C, and the acid chloride (1.2 equiv) was added. The mixture was left to stir at room temperature for 4 h. Water (20 mL) was added, and undissolved solids were filtered off. The filtrate was then extracted with ether (30 mL) and washed with sat. $CuSO_4$(aq) (3 × 10 mL), water (3 × 10 mL), and $NaHCO_3$(aq) (3 × 10 mL). This was followed by drying with $MgSO_4$ and removal of the solvent under reduced pressure. The crude product was then recrystallized.

Trichloroacetate 11. mp 78−79 °C, ^{1}H NMR δ ($CDCl_3$) 7.42−7.14 (8H,m); 5.31 (1H, ddd, J = 3 Hz, 3 Hz, 9 Hz); 4.73 (1H, d, J = 3 Hz); 4.39 (1h, dd, J = 3 Hz, 3 Hz); 2.46 (1H, ddd, J = 3 Hz, 9 Hz, 13.5 Hz); 1.73 (1H, ddd, J = 3 Hz, 3 Hz, 13.5 Hz). ^{13}C NMR δ ($CDCl_3$); 161.52; 143.70, 142.63, 138.39, 137.97; 126.88, 126.54, 126.14, 125.98, 125.91, 125.26, 123.43, 123.19; 77.57; 48.03; 43.32; 35.41.

Methanesulfonate 12. mp (methanol) 123−124 °C,^{1}H NMR δ ($CDCl_3$) 7.40−7.11 (8H, m); 5.13 (1H, ddd, J = 3 Hz, 3 Hz, 9 Hz); 4.72 (1H, d, J = 3 Hz); 4.32 (1H, dd, J = 3 Hz, 3 Hz); 2.94 (3H, s); 2.44 (1H, ddd, J = 3 Hz, 9 Hz, 13.5 Hz); 1.75 (1H, ddd, J = 3 Hz, 3 Hz, 13.5 Hz). ^{13}C NMR δ ($CDCl_3$): 143.47; 142.86; 138.42; 137.85; 126.94; 126.56; 126.18; 126.14; 125.33; 123.44; 123.23; 78.42; 49.67; 43.26; 38.61; 35.98.

Benzoate 13. mp 145−145.5 °C, ^{1}H NMR δ ($CDCl_3$) 8.20 (2H, dd, J = 1.5 Hz, 8 Hz); 7.84−7.15 (13H, m); 5.41 (1H, ddd, J = 3 Hz, 3 Hz, 8.8 Hz); 4.71 (1H, d, J = 3 Hz); 4.39 (1H, dd, J = 3 Hz, 3 Hz); 2.50 (1H, ddd, J = 3 Hz, 8.7 Hz, 13.2 Hz); 1.71 (1H, ddd, J = 3 Hz, 3 Hz, 13.2 Hz). ^{13}C NMR δ ($CDCl_3$) 166.12; 143.85; 143.17; 139.39; 139.31; 134.45; 132.78; 130.49; 129.39; 128.80; 128.17; 125.93; 125.87; 125.59; 125.09; 123.33; 123.18; 72.79; 48.83; 43.66; 36.17.

***p*-Nitrobenzoate 15.** mp 148−149C (from methanol). ^{1}H NMR δ ($CDCl_3$); 8.20 (2H, d, J = 8.7 Hz); 7.92 (2H, d, J = 8.7 Hz); 7.41−7.13 (8H, m); 5.42 (1H, ddd, J = 3 Hz, 3 Hz, 8.7 Hz); 4.70 (1H, d, J = 3 Hz); 4.40 (1H, dd, J = 3 Hz, 3 Hz); 2.50 (1H, ddd, J = 3 Hz, 8.7 Hz, 13.5 Hz); 1.70 (1H, ddd, J = 3 Hz, 3 Hz, 13.5 Hz). ^{13}C δ ($CDCl_3$) 164.23; 150.48; 143.80, 143.09, 139.07, 138.97; 135.66; 130.52; 126.80, 126.48, 126.11, 126.04, 125.49, 125.21; 123.4; 73.88; 48.74; 43.64; 36.24.

3,5-Dinitrobenzoate 16. mp 197−198 °C, ^{1}H NMR δ ($CDCl_3$): 9.15 (1H, dd, J = 2 Hz, 2 Hz); 8.84 (2H, d, J = 2 Hz); 7.42−7.14 (8H, m); 5.46 (1H, ddd, J = 3 Hz, 3 Hz, 9 Hz); 4.72 (1H, d, J = 3 Hz); 4.42 (1H, dd, J = 3 Hz, 3 Hz); 2.52 (1H, ddd, J = 3 Hz, 9 Hz, 13.5 Hz); 1.73 (1H, ddd, J = 3 Hz, 3 Hz, 13.5 Hz). ^{13}C NMR δ ($CDCl_3$) 161.97; 148.54; 143.75, 142.77, 138.75, 138.46; 133.99; 129.23; 126.94, 126.76, 126.30, 126.19, 125.37, 125.29, 123.63, 123.47; 122.23; 74.97; 48.66; 43.49; 36.38.

4-Nitrophenoxide 14. A suspension of sodium hydride (1.5 mmol) in anhydrous THF (5 mL) was treated with a solution of alcohol (MM) (0.10 g, 0.45 mmol) in dry THF (15 mL). The resulting solution was stirred at RT for 2 h. A solution of *p*-fluoronitrobenzene (0.09 g, 0.64 mmol) in dry THF (5 mL) was added slowly and the reaction left stirring for 40 h. Excess sodium hydride was destroyed by the careful addition of water, and the resulting mixture was extracted with ether (30 mL). The ether layer was washed with water (3 × 10 mL), dried ($MgSO_4$), and evaporated under reduced pressure to give a solid which was recrystallized from methanol giving **14** (0.12 g, 74%). mp (methanol) 182−183 °C, ^{1}H NMR δ ($CDCl_3$) 8.17 (2H, d, J = 9.3 Hz); 7.40−7.17 (8H, m); 6.83 (2H, d, J = 9.3 Hz); 4.82 (1H, ddd, J = 3 Hz, 3 Hz, 9 Hz); 4.67 (1H, d, J = 3 Hz); 4.40 (1H, dd, J = 3 Hz, 3 Hz); 2.49 (1H, ddd, J = 3 Hz, 9 Hz, 3 Hz); 1.68 (1H,ddd, J = 3 Hz, 3 Hz, 13 Hz). ^{13}C NMR δ ($CDCl_3$); 162.58; 143.69, 142.91; 141.33; 139.16, 138.62; 126.72, 126.32, 126.03, 125.91, 125.70, 124.84, 123.47, 123.12, 115.42; 76.17; 48.74; 43.58; 36.12.

Acknowledgment. Our grateful thanks to the ARC for financial support and for an APRA scholarship for one of us (B.R.P.), and the MARC Centre of the University of Melbourne for access to a farm of DEC workstations through a RAS grant. Thanks also go the referees for some very helpful comments and to Dr. J. Lawlor (this department) for help in preparing this manuscript.

Supporting Information Available: Includes details of the X-ray structural analyses including atomic coordinates, bond distances, angles, dihedral angles, and thermal ellipsoid plots, and *z* matrices for all the ab initio calculations. This material is available free of charge via the Internet at http://pubs.acs.org.

JO0055638